NATIONAL ADVISORY COMMITTEE FOR AERONAUTICS

TECHNICAL NOTE 4301

EFFECTS OF BOUNDARY-LAYER DISPLACEMENT AND LEADING-EDGE BLUNTNESS ON PRESSURE DISTRIBUTION, SKIN FRICTION, AND HEAT TRANSFER OF BODIES AT HYPERSONIC SPEEDS

By Mitchel H. Bertram and Arthur Henderson, Jr.

Langley Aeronautical Laboratory
Langley Field, Va.

Washington
July 1958

ERRATA

NACA TN 4301

By Mitchel H. Bertram and Arthur Henderson, Jr.
June 1958

Page 3, line 5:

Change symbol Δp_Λ to p_Λ and revise definition as follows:

p_Λ local pressure due to blunting with sweep

Pages 8 and 9:

Replace the section "Effect of sweep on surface pressures" beginning with line 16 on page 8 and ending with line 3 on page 9 with the following revised section:

Effect of sweep on surface pressures.- The effect of sweep on the blunt-leading-edge induced pressures is also of considerable practical significance. Sweep has been investigated by again resorting to blast-wave theory and assuming that the induced pressures are a function only of the cross-flow component of the Mach number. At zero angle of attack the induced pressure at a given streamwise location on a wing with sweep is found to be reduced from the pressure on an unswept wing by a factor equal to the cosine of the sweep angle to the 4/3 power. This relationship is shown in figure 10. The effects of sweep can be considerable; for example, at a sweep angle of 60° the induced pressures are predicted to be about 40 percent of those for zero sweep.

Figure 11 presents the pressure data for the hemicylinder-leading-edge plate at zero angle of attack at $M_\infty = 6.9$ in a form designed to test this prediction of the effect of sweep. The pressure ratio modified by the cosine function is plotted against streamwise distance in terms of nose thickness. The cosine function is found to correlate the pressure data for 0° and 40° sweep with good accuracy. However, the data for 60° of sweep are about 30 percent higher than the data for the two lower sweep angles. This discrepancy is roughly that which would be expected were viscous effects present, inasmuch as the cosine function is not a correlating factor for viscous effects. The agreement with theory, from the sonic-wedge leading-edge correlation by blast-wave theory presented earlier, is considered good.

Issued May 8, 1959

The effect of sweep at an angle of attack of 5° is shown in figure 12. Again the cosine function correlates the pressures for 0° and 40° sweep on each side. Here the pressure is presented as the increment in pressure due to the blunt leading edge. The positive values of $\alpha = 5^{\circ}$ refer to the windward side of the plate, whereas the values of $\alpha = -5^{\circ}$ refer to the leeward side. The exception to the correlation for the 60° swept plate is probably due in part to the viscous effects previously mentioned and in part to the fact that the asymptotic behavior of the pressure function used is incorrect at low pressures, since the cosine-function correlation assumes that the induced pressure ratios are large.

Pages 24, 25, 26:

Replace these pages with corrected pages 24, 25, and 26 attached. Note that on page 24 only figure 10 has been revised, but the complete page is reproduced as a matter of convenience.

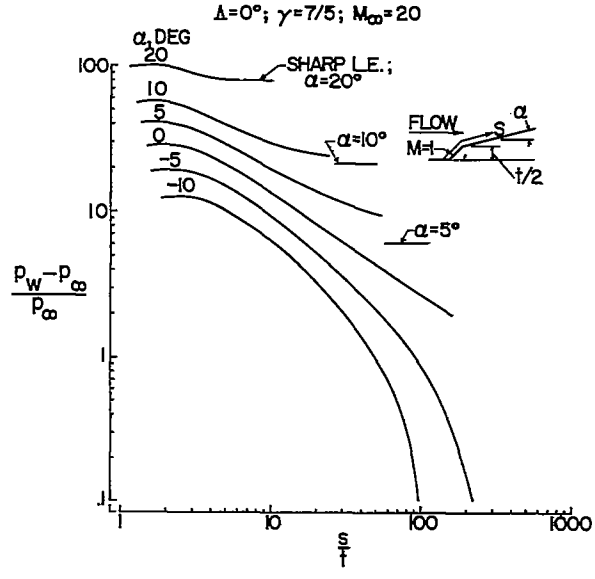

Figure 9.- Effect of α on blunt-leading-edge induced pressures on a flat plate.

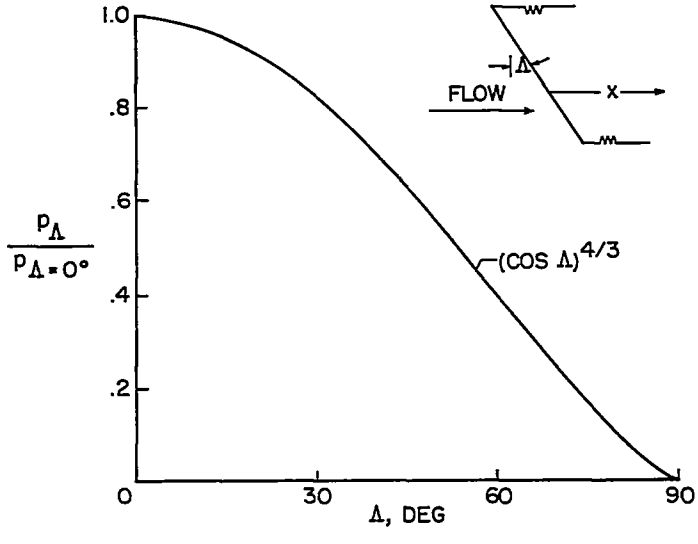

Figure 10.- Effect of leading-edge sweep on blunt-leading-edge induced pressures. $\alpha = 0^{\circ}$.

Issued May 8, 1959
Page 3 of 5 pages

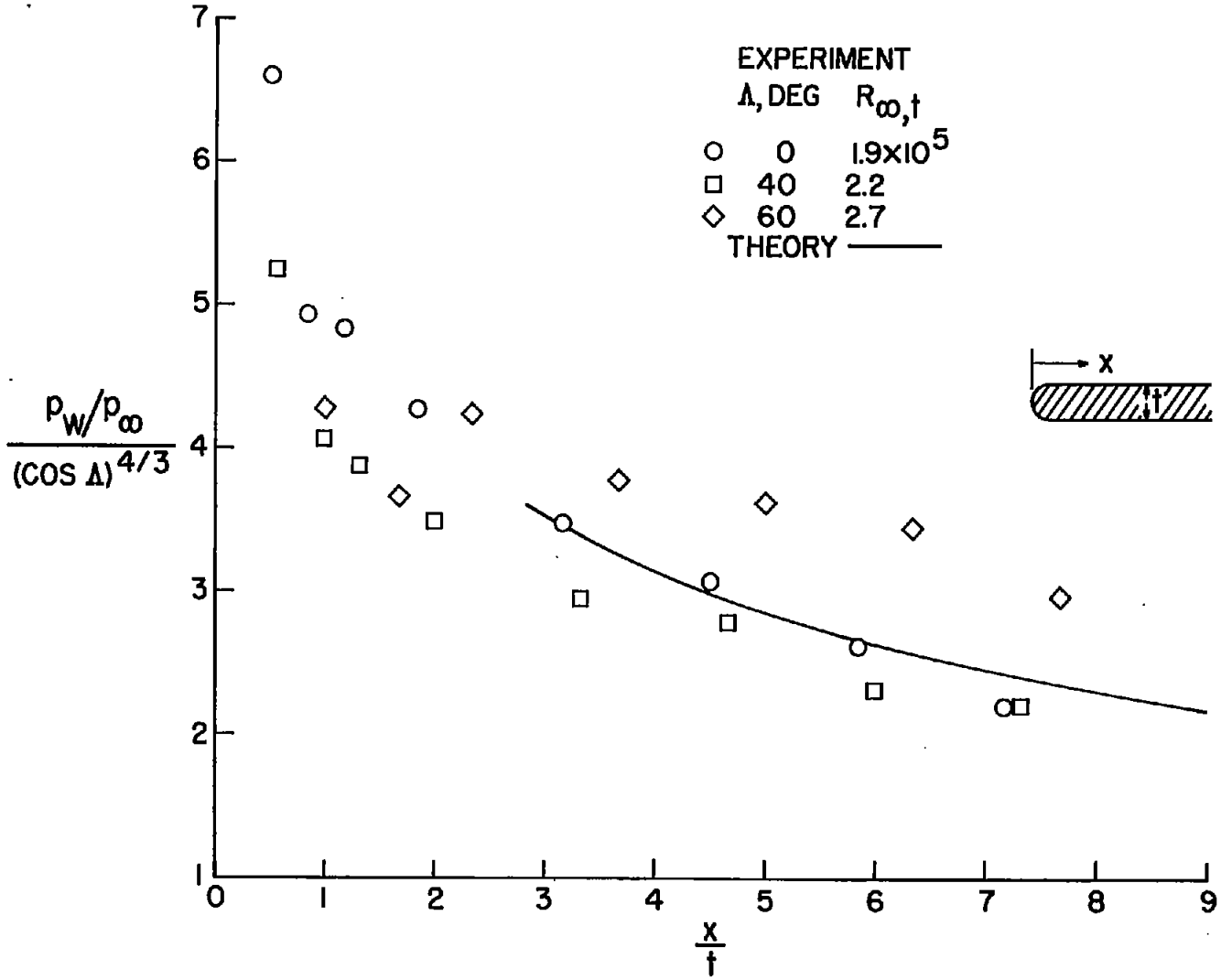

Figure 11.- Correlation of pressures on a flat plate with a hemicylinder leading edge tested in air. $\alpha = 0°$; $M_\infty = 6.9$.

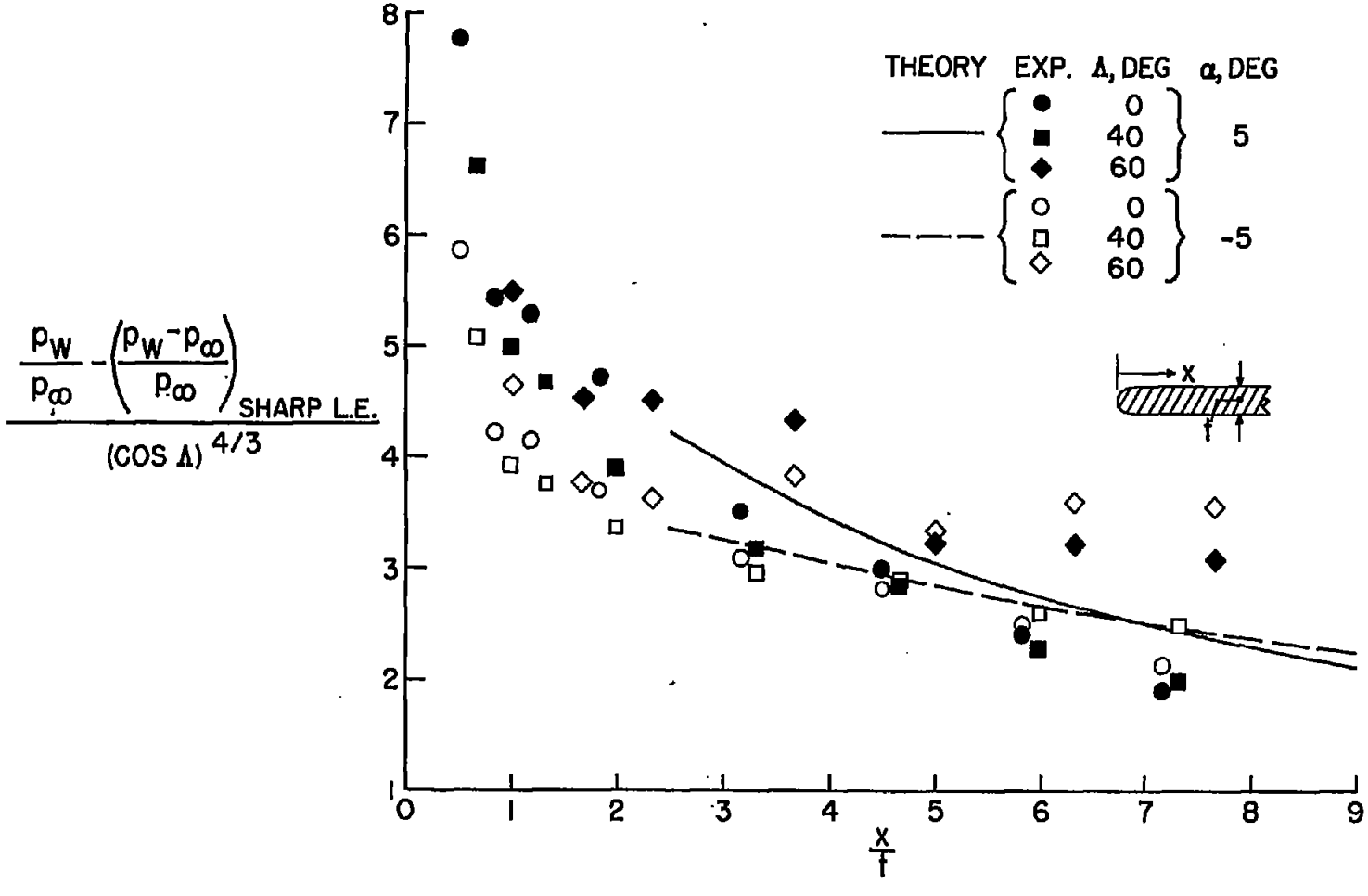

Figure 12.- Effect of sweep on pressures on a flat plate with hemi-cylinder leading edge tested in air.

NATIONAL ADVISORY COMMITTEE FOR AERONAUTICS

TECHNICAL NOTE 4301

EFFECTS OF BOUNDARY-LAYER DISPLACEMENT AND LEADING-EDGE BLUNTNESS ON PRESSURE DISTRIBUTION, SKIN FRICTION, AND HEAT TRANSFER OF BODIES AT HYPERSONIC SPEEDS

By Mitchel H. Bertram and Arthur Henderson, Jr.

SUMMARY

Results are presented of an investigation to determine the effect of boundary-layer displacement and leading-edge bluntness on surfaces in hypersonic flow. The presence of the boundary layer and the blunt leading edge induce pressure gradients which in turn affect the skin friction and heat transfer to the surface. Methods for predicting these phenomena on two-dimensional surfaces are given and a brief review of recent three-dimensional results is presented.

INTRODUCTION

In hypersonic flow large pressure and temperature gradients can be induced on a plate without the plate itself having an inclination. In pure form two main types of induced effects may be detected. One is the pressure gradient induced by the presence of thick boundary layers on sharp leading-edge plates and the other is the pressure gradient induced on surfaces following very blunt leading edges. These induced effects, together with the manner in which they are influenced by plan form and angle of attack, are the main consideration of this investigation. In addition, since purity is not often attained and the cases in which the two induced effects act simultaneously are often of more practical significance, the case of mixed effects is also considered. The important progress that has been made in these areas is demonstrated.

SYMBOLS

a'	skin-friction constant in viscous-interaction theory
A	aspect ratio

C_c chord-force coefficient

$\overline{C}_{c,p}$ inviscid pressure chord-force coefficient

$\Delta C_{c,p}$ increment in pressure chord-force coefficient due to boundary-layer-displacement effects

$C_{c,t}$ pressure-chord-force-coefficient contribution due to finite thickness of leading edge

$C_{D,N}$ nose drag coefficient based on forward projected area of nose

C_F average skin-friction coefficient for one side of flat plate including boundary-layer-displacement effects

ΔC_F increment in average skin-friction coefficient due to boundary-layer-displacement effects

$\overline{C}_{F,T}$ total skin-friction coefficient of flat plate with zero pressure gradient

$C_{F,T}$ total skin-friction coefficient of flat plate including boundary-layer-displacement effects

$C_\mu = \frac{\mu_w T_\infty}{\mu_\infty T_w}$

$C_{\mu,e} = \frac{\mu_e T_\infty}{\mu_\infty T_e}$

C_{N_α} flat-plate normal-force-curve slope including boundary-layer-displacement effects

$\overline{C}_{N_\alpha}$ flat-plate normal-force-curve slope (inviscid)

d nose diameter

L plate length

M_∞ free-stream Mach number

M_a asymptotic Mach number on flat plate (inviscid sharp-leading-edge value)

h	heat-transfer coefficient including pressure-gradient effects
$\bar{h}$	heat-transfer coefficient with zero pressure gradient
$N_{St,\infty}$	Stanton number based on free-stream conditions
p	local pressure
Δp_{Λ}	local pressure rise due to blunting with sweep
p_{∞}	free-stream pressure
p_a	asymptotic pressure on flat plate (inviscid sharp-leading-edge value)
p_c	theoretical inviscid pressure on cone surface
p_w	surface pressure
$R_{a,x}$	Reynolds number based on asymptotic conditions on flat plate (inviscid sharp-leading-edge values)
$R_{\infty,c}$	Reynolds number based on free-stream conditions and root chord of delta wing
$R_{\infty,d}$	Reynolds number based on free-stream conditions and nose diameter
$R_{\infty,t}$	Reynolds number based on free-stream conditions and nose thickness
$R_{\infty,x}$	Reynolds number based on free-stream conditions and streamwise distance
R_S	Reynolds number based on sharp-cone surface conditions and surface distance from the nose
S	distance along surface
t	nose thickness
T_e	recovery temperature

T_w	wall temperature
T_0	stagnation temperature
x	streamwise distance along axis
α	angle of attack
δ	plate deflection angle
Λ	sweepback angle
γ	ratio of specific heats
μ_w	dynamic viscosity at wall temperature
μ_e	dynamic viscosity at recovery temperature
$\bar{\chi}_\infty$	viscous interaction parameter based on free-stream conditions, $M_\infty^3\sqrt{C_\mu}/\sqrt{R_{\infty,x}}$
$\bar{\chi}_{\infty,S}$	viscous interaction parameter based on free-stream conditions and using the square root of the plate area as the characteristic length in the Reynolds number

RESULTS FOR TWO-DIMENSIONAL CONFIGURATIONS

Boundary-Layer-Displacement Effects

Surface pressures.- The effect of the boundary layer in displacing the flow around flat plates is most familiar through its effect on the pressure distribution. Recently high Mach number data have become available for pressure distributions on flat plates with very sharp leading edges. Published data of this type are given in references 1 and 2. More recent data are given by some measurements in the Mach number 9.6 nozzle of the Langley 11-inch hypersonic tunnel to test both changes in Reynolds number and angle of attack shown in figure 1. These results were obtained with, for this setup, an unavoidable heat transfer. The abscissa in figure 1 is a parameter first shown by Lees and Probstein (ref. 3) to be that for which correlation of boundary-layer induced effects should be obtained. In it Mach number, Reynolds number, and coefficient in the linear formula for viscosity are used at the local asymptotic flow conditions, that is, the conditions that would be

obtained on the plate at each angle of attack were there no boundary layer present. Also the viscosity coefficient C_{μ} is evaluated at estimated recovery conditions designated $C_{\mu,e}$. The pressure parameter in the ordinate is the pressure rise above asymptotic pressure divided by the asymptotic pressure.

Large pressure rises are obtained as the leading edge is approached. Although all the angles of attack correlate well, the original data (the open symbols) fall below the line given by insulated-plate theory (Lees' first-order strong interaction, ref. 4) due to heat transfer from the boundary layer to the plate wall during these transient tests. The inset in figure 1 shows the measured temperatures along the plate normalized with respect to stagnation temperature, together with the polynomial fitted to these data for use with the theoretical method of modifying the data to insulated-plate conditions. In the same manner that was found to be successful in reference 2, the original data were modified to the insulated-plate case. The result is shown by the solid symbols in figure 1 and is in general agreement with the theoretical line.

Skin friction.- These large pressures, of course, have an effect on both skin friction and heat transfer. The results of strong-interaction theory and the hypersonic equations for pressure as a function of plate deflection angle are used to obtain figure 2, which shows the contribution of each surface of a two-dimensional wedge wing to the total skin friction. This contribution of each surface is normalized with respect to the total skin friction of a flat-plate wing (both surfaces) with a zero pressure gradient at zero angle of attack. The hypersonic boundary-layer-interaction parameter is evaluated at undisturbed free-stream conditions ahead of the plate. So long as the wall temperature is constant the plot is independent of the wall temperature. The constant a' is a function of wall temperature and is tabulated and plotted graphically in reference 2. When $\bar{\chi}_{\infty} = 0$, the classical flat-plate skin-friction values result.

Utilizing these same equations but adapting them to the delta wing according to reference 2 permits a similar plot to be constructed for a delta wing. Such a plot is shown in figure 3. For the delta wings the Reynolds number utilizes the square root of the projected wing area as the characteristic length. This is done to facilitate the use of area as a comparison basis.

As an illustration of the use of the results from figures 2 and 3, figure 4 has been prepared. Figure 4 gives the total skin friction for a two-dimensional and a delta-plan-form flat plate as a function of the hypersonic similarity parameter for various values of the

hypersonic interaction parameter. Of course, a similar plot can be constructed for a wing of given wedge angle from figures 2 and 3. Note the appreciable increases in total skin friction due to boundary-layer-displacement effects, even at moderate values of the hypersonic interaction parameter.

Both flat-plate and delta-wing data for skin friction at $M_\infty = 6.8$ have been presented in reference 2. The magnitude of the increase in skin friction which could be ascribed to boundary-layer-displacement effects was correctly predicted. Recent data obtained at Mach number 9.6 for the variation of chord force with angle of attack for a delta-wing—half-cone combination obtained by W. O. Armstrong in the Langley 11-inch hypersonic tunnel are shown in figure 5. For the present purposes the presence of the half-cone complicates but need not obscure the comparison. The lines at the bottom of this figure outline the various contributions to the pressure chord force such as the inviscid-pressure chord force $(C_{c,p})$, the increment in pressure chord force due to boundary-layer-displacement effects $(\Delta C_{c,p})$, and the leading-edge-thickness contribution to the chord force $(C_{c,t})$. The large area immediately above the pressure contributions is the skin friction for a delta-plan-form flat plate with zero pressure gradient $(\bar{C}_F)$, and the area above this (designated ΔC_F) is the increment in skin friction calculated to be due to boundary-layer-displacement effects. This increment alone is, in general, larger than the pressure drag from all sources on this model. Because of the shielding effect on the cone, the negative angles of attack are relied upon for comparison between theory and experiment. Throughout the entire range, however, the prediction of theory is considered good.

Normal force.- The results discussed have been concerned with the effect on the skin friction attributable to boundary-layer displacement; however, there is a corresponding effect on the normal force, so that the L/D of the wing is probably less affected than would be indicated by displacement effects on skin friction alone. The predicted effect on normal force for a two-dimensional insulated flat plate is compared in figure 6 with data obtained by Tellep in the University of California low-density tunnel at a Mach number of about 4 (ref. 5). Shown are Tellep's original data for various aspect ratios and the data modified to infinite aspect ratio according to Tellep. The increases in normal force can be large, and one factor illustrated in figure 6 is the need of more attention to the effect of aspect ratio.

Blunt-Leading-Edge Effects

Blast-wave theory correlation of surface pressures at zero sweep and zero angle of attack.- Thus far, only the viscous or boundary-layer induced effects have been treated. As mentioned previously, the conditions on a plate with a blunt leading edge represent another example of an induced effect that assumes significance at hypersonic speeds. The increase in pressures on a plate following a blunt leading edge has been known for some time and has been demonstrated both theoretically and experimentally (refs. 6 to 8). Cheng and Pallone (ref. 9) and Lees and Kubota (ref. 10) more recently have given the proper correlating parameters for this phenomenon. Their work stems from the so-called "blast-wave" theory in which the two-dimensional blunt leading edge is taken as the origin of an explosion in which the energy released is proportional to the leading-edge drag. The theoretically predicted correlation parameter has been found to correlate the results from characteristics theory where a sonic wedge is utilized as the blunt leading edge (ref. 11). This correlation of surface pressures over an extended range of Mach number in air and helium is shown in figure 7. The correlation parameter from blast-wave theory is the abscissa in the figure. This correlation parameter combines the effect of distance from the leading edge, Mach number, and nose drag. The ordinate is the nondimensionalized wall pressure rise above free-stream pressure induced by the blunt leading edge. The correlation is good except very near the nose (within the first 3 to 4 nose diameters) where the theory is not expected to apply. First-order blast-wave theory is also shown on this plot. Note the departure of this theory from the characteristics solutions at large values of x/t. This first-order blast-wave theory again is not expected to apply at these larger values of the distance parameter.

Effect of angle of attack on surface pressures at zero sweep.- For comparison of the theory with experiment, Princeton helium-tunnel data obtained at $M_\infty = 11.4$ with viscous effects believed to be negligible have been utilized, and the data were found to be in reasonable agreement with theory (ref. 11). Some recent data bearing on this problem have been obtained by W. V. Feller on a hemicylinder leading-edge plate in the Langley 11-inch hypersonic tunnel. Although the Mach number is somewhat low $(M_\infty = 6.9)$ a number of test variables are covered, and for this reason the data are valuable. Experimental and theoretical data for the zero-yaw plate are presented in figure 8 for several angles of attack. The ordinate in this figure is the increment in pressure ratio due to the blunt leading edge at each angle of attack. A positive angle of attack refers to the windward surface of the plate, while a negative angle of attack indicates the leeward or shielded side of the plate. The abscissa is distance from the leading edge in terms of leading-edge thickness. The theoretical

lines are the result of the characteristics solutions for the sonic-wedge leading-edge plate. Note that the trend with angle of attack is well predicted by theory.

In order to determine trends to be expected from similar results at a higher Mach number, figure 9 has been prepared from characteristics solutions for the flat plate with sonic-wedge leading edge at a Mach number of 20. This figure presents the pressure rise on the wing surface due to a combination of angle of attack and leading-edge bluntness as a function of surface distance. The rise in pressure above the asymptotic pressure (the sharp-leading-edge plate pressure) is considerably reduced, percentagewise, as the angle of attack is increased. Note the large induced pressures, especially on the low-pressure side of the plate. At $\alpha = -10^\circ$, pressure-difference ratios as high as the order of 10 are predicted while the inviscid pressure for a sharp-leading-edge plate is essentially zero absolute.

Effect of sweep on surface pressures.- The effect of sweep on the blunt-leading-edge induced pressures is also of considerable practical significance. Sweep has been investigated by again resorting to blast-wave theory and assuming that the induced pressures are a function only of the cross-flow component of the Mach number. At zero angle of attack the induced-pressure rise at a given streamwise location on a wing with sweep is found to be reduced from the pressure rise on an unswept wing by a factor equal to the cosine of the sweep angle to the 8/3 power. This relationship is shown in figure 10. The effects of sweep can be large; for example, at a sweep angle of 60° the induced-pressure rises are predicted to be about 1/7 of those for zero sweep.

Figure 11 presents the pressure data for the hemicylinder-leading-edge plate at zero angle of attack at $M_\infty = 6.9$ in a form designed to test this prediction of the effect of sweep. The pressure rise modified by the cosine function is plotted against streamwise distance in terms of nose thickness. The cosine function is found to correlate the pressure-rise data for 0° and 40° sweep with excellent accuracy. However, the data for 60° sweep are about 15 percent higher than the data for the two lower sweep angles. This discrepancy is that which would be expected were viscous effects present, inasmuch as the cosine function is not a correlating factor for viscous effects. The agreement with theory, from the sonic-wedge leading-edge correlation by blast-wave theory presented earlier, is considered good.

The effect of sweep at an angle of attack of 5° is shown in figure 12. Again the cosine function correlates the pressures for each side. Here again the pressure is presented as the increment in pressure due to the blunt leading edge. The positive values of $\alpha = 5^\circ$

refer to the windward side of the plate while -5° refers to the leeward side. The main exception to correlation is for the 60° swept plate on the leeward side.

Combined Viscous and Leading-Edge-Bluntness Effects

Thus far, the viscous and blunt-leading-edge effects have been treated separately. In actual applications, however, they will probably more often than not be found to be acting simultaneously. A fair amount of pressure data of this type has been obtained in the Princeton helium tunnel (refs. 8 and 12). Recently pressure data of this mixed viscous and blunt-leading-edge type have been obtained on a flat plate in a 2-inch helium jet at the Langley Laboratory, in which the available data are extended to very high Mach numbers (Mach numbers in the range 17 to 23). Some Princeton data are shown in figure 13(a) and some Langley data in figure 13(b). By choice, the pressure-rise parameter has been plotted against the viscous-correlation parameter. For clarity only the highest and lowest Mach numbers and Reynolds numbers for the Langley tests have been shown. A simple linear addition of the pressure predictions of viscous theory and sonic-wedge characteristics theory modified according to blast-wave theory is presented for comparison with the data. The viscous theory was obtained by the method of reference 13 with a continuously variable Mach number gradient. There is no large consistent disagreement between theory and experiment. The very large pressure rises that can be obtained on a flat plate at zero angle of attack from a combination of viscous and blunt-leading-edge effects should be noted.

Heat Transfer

The next problem to be considered is that of heat transfer to these surfaces. A simple solution to the problem of laminar heat transfer to surfaces on which pressure gradients occur in hypersonic flow is available from similarity theory. This solution which is restricted to power-law variations of pressure with surface distance was pointed out by Li and Nagamatsu (ref. 14), who worked out in detail the case of the strong-interaction self-induced pressure gradient by this method. M. H. Bertram of the Langley Laboratory has determined the results from this solution for general use. The result for heat transfer is shown in figure 14, where $\bar{h}$ represents the local heat-transfer coefficient with zero pressure gradient at the reference pressure level p_∞ and h represents the local heat-transfer coefficient including the effect of pressure gradient at the local pressure level p_w. Note that the pressure gradient

reduces the heat transfer but a high local pressure increases the heat transfer. The value of $n = -0.875$ corresponds to infinitely favorable velocity gradient in the transformed plane with $\gamma = 7/5$.

This theory has been utilized for comparison with some available data, namely, that of Crawford and McCauley (ref. 15) and Creager (ref. 16) shown in figure 15. Crawford and McCauley's data were obtained on hemisphere-nosed cylinder at Mach number 6.8. For purpose of analysis, these data were assumed to be equivalent to flat-plate data. Creager's data were obtained on a hemicylinder-leading-edge flat plate at zero angle of attack and Mach number 3.9. In order to obtain the curves from similarity theory, power laws were fitted to the measured pressure distributions. In general, good fits to the pressure data could be obtained. The exception was Creager's pressure data which at the higher values of x/t showed a variation of pressure with inverse distance higher than the 2/3 power so that lateral and trailing-edge effects were indicated. Thus, for these data only the lower values of x/t were theoretically evaluated. The correlation parameter for laminar theory $N_{St,\infty}\sqrt{R_{\infty,x}}$ is plotted in figure 15 against the streamwise distance in terms of nose thicknesses. The data from reference 15 and from reference 16 (in the range considered) are found to be well predicted by similarity theory. These pressure-gradient effects will of course assume greater importance at very high Mach numbers where the induced pressures are much larger.

THREE-DIMENSIONAL CONFIGURATIONS

Pressures on Blunted Rods

In the discussion of the effects considered thus far, three-dimensional bodies in general have not been considered. A short review of some recent results on simple bodies at high Mach numbers will now be presented. In figure 16 are shown surface-pressure results from blunt-nose rods immersed in hypersonic helium flow. Data from two sources are shown: results from the Princeton helium tunnel (ref. 17) and unpublished results from the Langley 2-inch helium jet. The pressure-rise parameter is shown plotted against the blast-wave-theory correlating parameter for a given nose shape, that is, distance (in rod diameters) divided by Mach number squared. In figure 16(a) are the results for the hemisphere tipped rod. These data appear to separate into two main groups; one, the Mach number 12 to 14 data, the other the Mach number 17 to 21 data. From flat-plate calculations based on the Mach number 21 data, the difference between the two sets of data appears, roughly, to be attributable to boundary-layer-displacement effects.

The data for the flat-nosed rod in figure 16(b) show somewhat better correlation at the higher values of x/d, although the Mach number 11.7 data are somewhat lower than the rest of the data. At the low value of x/d the familiar phenomenon of overexpansion around the 90° corner is noted.

Pressures on Blunted Cones

A next step in this study is to investigate a blunt-nosed body with finite afterbody angle. Pressure measurements have been obtained on a flat-nosed 10° half-angle cone in a 2-inch helium jet at the Langley Laboratory. These results are shown in figure 17 for Mach numbers of 17 and 23 and various nose diameter Reynolds numbers. The pressure change from inviscid sharp-cone pressure divided by the sharp-cone pressure is plotted against distance in nose diameters along the cone axis. Before the data are examined in detail, note the general level of the measured pressure rises, which are quite small compared with data from flat plates in both air and helium presented earlier in figures 1 and 13. The magnitude of these pressure changes is in tenths whereas the flat-plate pressure rises ranged from values as high as 10 to 40. The theory shown in figure 17 is Probstein's for hypersonic laminar-boundary-layer interaction over a cone (ref. 18). Only sharp cones are considered in the theory.

For the two lowest Reynolds numbers, the agreement of experiment with theory is considered good, that is, at least for the region beyond about 17 diameters of the nose. Here viscous effects appear to be dominant. However, the picture changes at the two highest Reynolds numbers. The inviscid flow field in the vicinity of the nose exerts its influence and the pressure distributions resemble those measured on flat-nosed cones in air at Mach number 6.85 (ref. 19) with a characteristic overexpansion in the region of 10 diameters which is qualitatively similar to the pressure distributions predicted by Chernyi (ref. 20). Viscous effects, though present, appear to be considerably modified or even subordinate to the inviscid flow field effects.

Heat Transfer to Sharp and Blunted Cones at $\alpha = 0°$

Heat-transfer data have been obtained in air at a free-stream Mach number of 6.7 on cones similar in configuration to those tested for surface pressures in helium. These cones had a 10° half-angle with sharp, flat, and tangent sphere tips. The tests were conducted at a stagnation temperature of about 1,120° R with a ratio of wall (essentially isothermal) to stagnation temperature close to 1/2. The experimentally determined recovery factor at $\alpha = 0°$ with laminar flow on a

thin-shell model of the sharp-tip cone was 0.843 (based on surface conditions). This value of recovery factor was used throughout in determining values of Stanton number from the temperature data.

Results at zero angle of attack are shown in figure 18. The ordinate is the laminar-heat-transfer correlation parameter in which Stanton number, Reynolds number R_S, and the coefficient in the linear formula for viscosity C_μ are evaluated at the theoretical surface conditions on the sharp-tip cone at zero angle of attack. The abscissa is the same Reynolds number used in the correlation parameter of the ordinate.

Although experimental values for the sharp-tip cone are somewhat higher than the laminar-theory values, the Stanton number parameter is essentially independent of the surface Reynolds number up to the Reynolds number at which the start of transition is indicated (about 4.5×10^6). When the tip of the cone is blunted, this insensitivity of the Stanton number parameter to Reynolds number no longer applies. There is a decided decrease in heat transfer relative to the heat transfer on the sharp-tip cone as the blunt tip is approached. The effect of blunting on the geometry alone (pressure assumed constant) when the Mangler transformation is used appears to account for substantially all of this decrease in heat transfer. In the theory the boundary layer is assumed to start two-dimensionally from the shoulder at the blunt nose and to approach the cone value asymptotically. Note that the blunt nose delays transition to surface Reynolds numbers of from 5×10^6 to 6×10^6.

Heat Transfer to Sharp and Blunted Cones at $\alpha = 5^\circ$

Next to be considered is the effect of angle of attack on the heat transfer to these cones. Shown in figure 19 are the heat transfers to the 0°, 90°, and 180° meridians of the sharp- and flat-faced cones at 5° angle of attack in the same Stanton number parameter form as were given the zero-angle-of-attack results. All parameters are normalized by or computed from the cone theory at zero angle of attack and thus are directly comparable to the zero-angle-of-attack results. As expected, the heat transfer over most of the length was highest along the most windward meridian (0°) and more or less continuously decreased to the top meridian (180°). The results at the side meridian (90°) were not greatly different from the zero-angle-of-attack results which are shaded in this figure. The effect of blunting is similar to that obtained at zero angle of attack. The most striking effect is that of angle of attack on transition and thus on the heat transfer to the 180° meridian. (Compare figs. 19(a) and 19(b).) Transition occurs

along this meridian first, and on the sharp cone (fig. 19(a)) the heat transfer becomes equal to or slightly higher than the heat transfer to the most windward meridian at the rearward stations (highest values of R_S). The 90° meridian has an increase in heat transfer well above the other two meridians at the most rearward station. Bluntness appears to delay transition along the 180° meridian, but the trend of the data appears to be much the same for the blunted cone as for the sharp-tipped cone. The initial points on the 180° meridian are believed to have a high indicated heat transfer because of lateral heat conduction, which was not taken into account in the analysis of the data since it was negligible in most instances.

CONCLUDING REMARKS

The results presented indicate that much of the viscous and nose-blunting phenomena that have been studied in the past in a rather academic way are now understood to the point where engineering estimates of many of their effects are now possible. However, a large area for additional research remains to be explored.

Langley Aeronautical Laboratory,
National Advisory Committee for Aeronautics,
Langley Field, Va., March 19, 1958.

REFERENCES

1. Kendall, James M., Jr.: An Experimental Investigation of Leading-Edge Shock-Wave - Boundary-Layer Interaction at Mach 5.8. Jour. Aero. Sci., vol. 24, no. 1, Jan. 1957, pp. 47-56.

2. Bertram, Mitchel H.: Boundary-Layer Displacement Effects in Air at Mach Numbers of 6.8 and 9.6. NACA TN 4133, 1958.

3. Lees, Lester, and Probstein Ronald F.: Hypersonic Viscous Flow Over a Flat Plate. Rep. No. 195 (Contract AF 33(038)-250), Aero. Eng. Lab., Princeton Univ., Apr. 1952.

4. Lees, Lester: Hypersonic Flow. Fifth International Aeronautical Conference (Los Angeles, Calif., June 20-23, 1955), Inst. Aero. Sci., Inc., 1955, pp. 241-276.

5. Tellep, D. M.: Lift on Flat Plates in Low Density Supersonic Flow. Rep. No. HE-150-131 (Ser. No. 20-104, Contract N7-onr-295-Task 3), Inst. Eng. Res., Univ. of California, Aug. 30, 1955.

6. Bertram, Mitchel H.: Viscous and Leading-Edge Thickness Effects on the Pressures on the Surface of a Flat Plate in Hypersonic Flow. Jour. Aero. Sci. (Readers' Forum), vol. 21, no. 6, June 1954, pp. 430-431.

7. McLellan, Charles H., Bertram, Mitchel H., and Moore, John A.: An Investigation of Four Wings of Square Plan Form at a Mach Number of 6.9 in the Langley 11-Inch Hypersonic Tunnel. NACA Rep. 1310, 1957. (Supersedes NACA L51D17.)

8. Hammitt, A. G., and Bogdonoff, S. M.: Hypersonic Studies of the Leading Edge Effect on the Flow Over a Flat Plate. Jet Propulsion, vol. 26, no. 4, Apr. 1956, pp. 241-246.

9. Cheng, H. K., and Pallone, A. J.: Inviscid Leading-Edge Effect in Hypersonic Flow. Jour. Aero. Sci. (Readers' Forum), vol. 23, no. 7, July 1956, pp. 700-702.

10. Lees, Lester, and Kubota, Toshi: Inviscid Hypersonic Flow Over Blunt-Nosed Slender Bodies. Jour. Aero. Sci., vol. 24, no. 3, Mar. 1957, pp. 195-202.

11. Bertram, M. H., and Baradell, D. L.: A Note on the Sonic-Wedge Leading-Edge Approximation in Hypersonic Flow. Jour. Aero. Sci. (Readers' Forum), vol. 24, no. 8, Aug. 1957, pp. 627-628.

12. Hammitt, Andrew G.: The Hypersonic Viscous Effect on a Flat Plate With Finite Leading Edge. Rep. No. 378 (WADC TN 57-105), Dept. Aero. Eng., Princeton Univ, Mar. 1957.

13. Bertram, Mitchel H.: An Approximate Method for Determining the Displacement Effects and Viscous Drag of Laminar Boundary Layers in Two-Dimensional Hypersonic Flow. NACA TN 2773, 1952.

14. Li, Ting-Yi, and Nagamatsu, H. T.: Hypersonic Viscous Flow on Non-insulated Flat Plate. Proc. Fourth Midwestern Conference on Fluid Mechanics, held at Purdue Univ. Sept. 8-9, 1955, Res. Ser. No. 128, Purdue Eng. Experiment Station, 1956, pp. 273-287.

15. Crawford, D. H., and McCauley, W. D.: Investigation of the Laminar Aerodynamic Heat-Transfer Characteristics of a Hemisphere-Cylinder in the Langley 11-Inch Hypersonic Tunnel at a Mach Number of 6.8. NACA Rep. 1323, 1957. (Supersedes NACA TN 3706, 1956.)

16. Creager, Marcus O.: Effects of Leading-Edge Blunting on the Local Heat Transfer and Pressure Distributions Over Flat Plates in Supersonic Flow. NACA TN 4142, 1957.

17. Vas, I. E., Bogdonoff, S. M., and Hammitt, A. G.: An Experimental Investigation of the Flow Over Simple Two-Dimensional and Axial Symmetric Bodies at Hypersonic Speeds. Rep. No. 382 (WADC TN 57-246), Dept. Aero. Eng., Princeton Univ., June 1957.

18. Probstein, Ronald F.: Interacting Hypersonic Laminar Boundary Layer Flow Over a Cone. Tech. Rep. AF 2798/1 (Contract AF 33(616)-2798), Div. Eng., Brown Univ., Mar. 1955.

19. Bertram, Mitchel H.: Tip-Bluntness Effects on Cone Pressures at M = 6.85. Jour. Aero. Sci., vol. 23, no. 9, Sept. 1956, pp. 898-900.

20. Chernyi, G. G.: Hypersonic Flow Around a Slender Blunt Cone. Morris Friedman Foreign Translations C-113. (From Doklady Akademii Nauk SSSR, vol. 115, no. 4, 1957, pp. 681-683.)

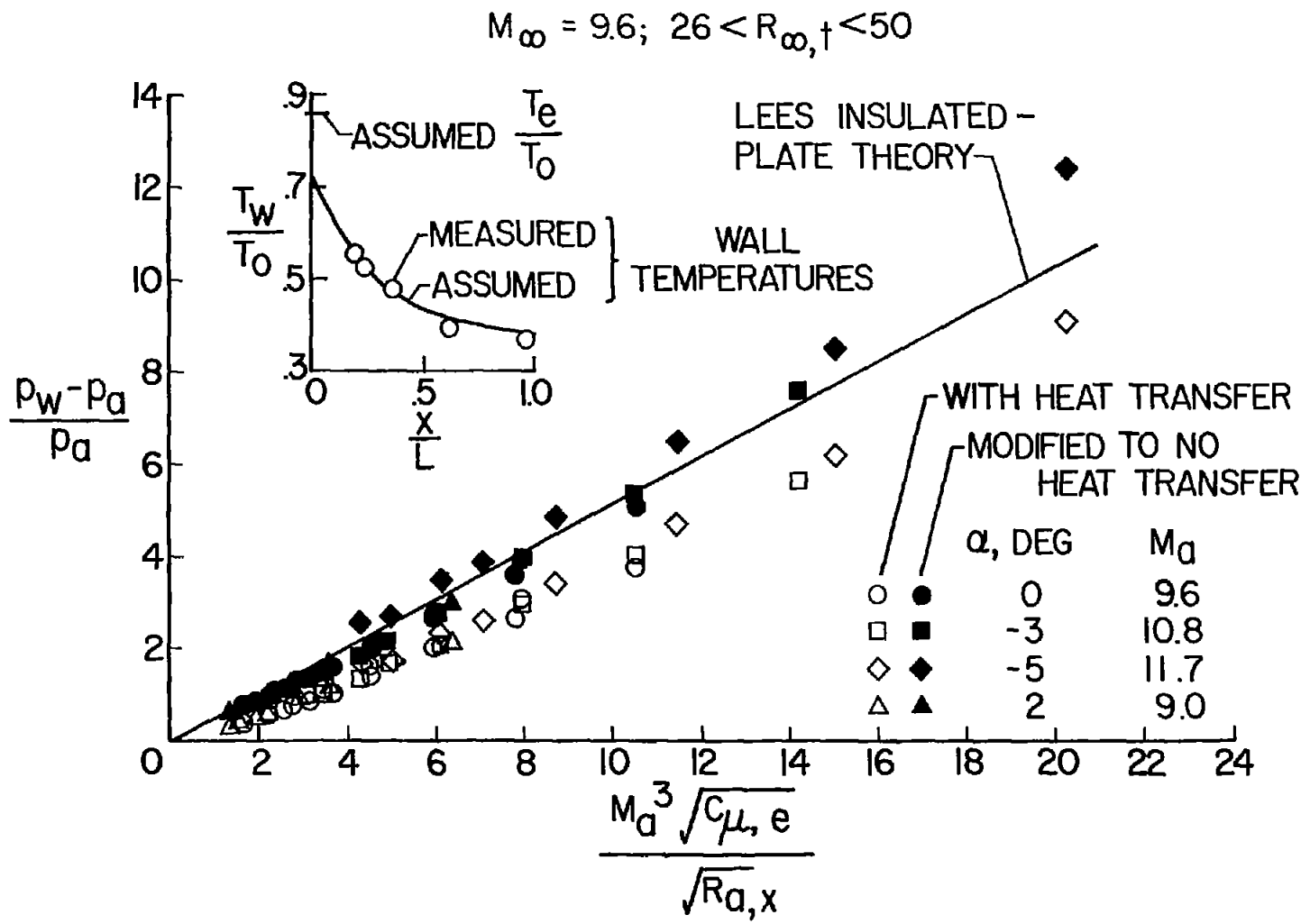

Figure 1.- Boundary-layer induced pressures on a flat plate tested in air.

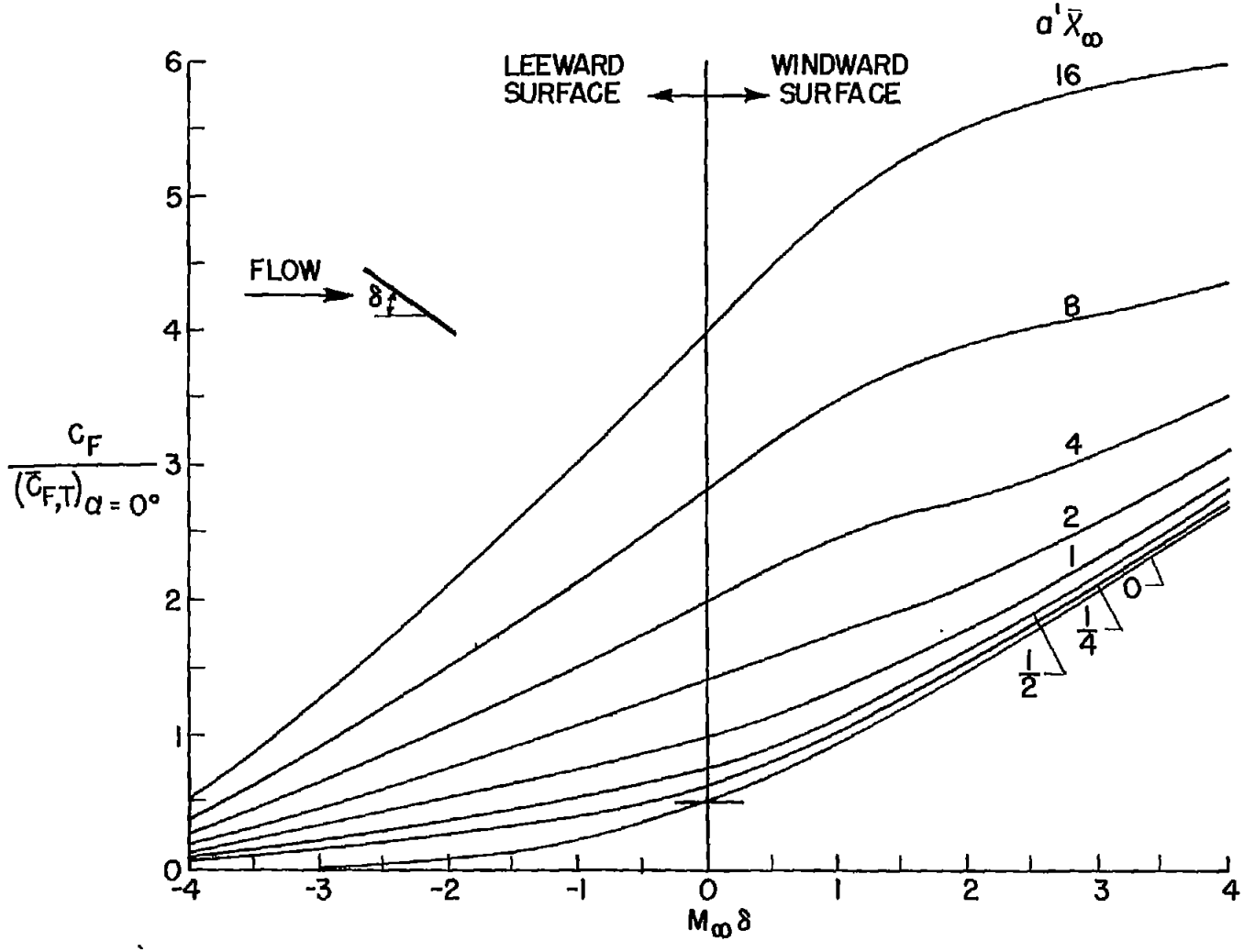

Figure 2.- Boundary-layer-induced and angle-of-attack effects on skin friction of a two-dimensional plan-form flat plate. $\gamma = \frac{7}{5}$.

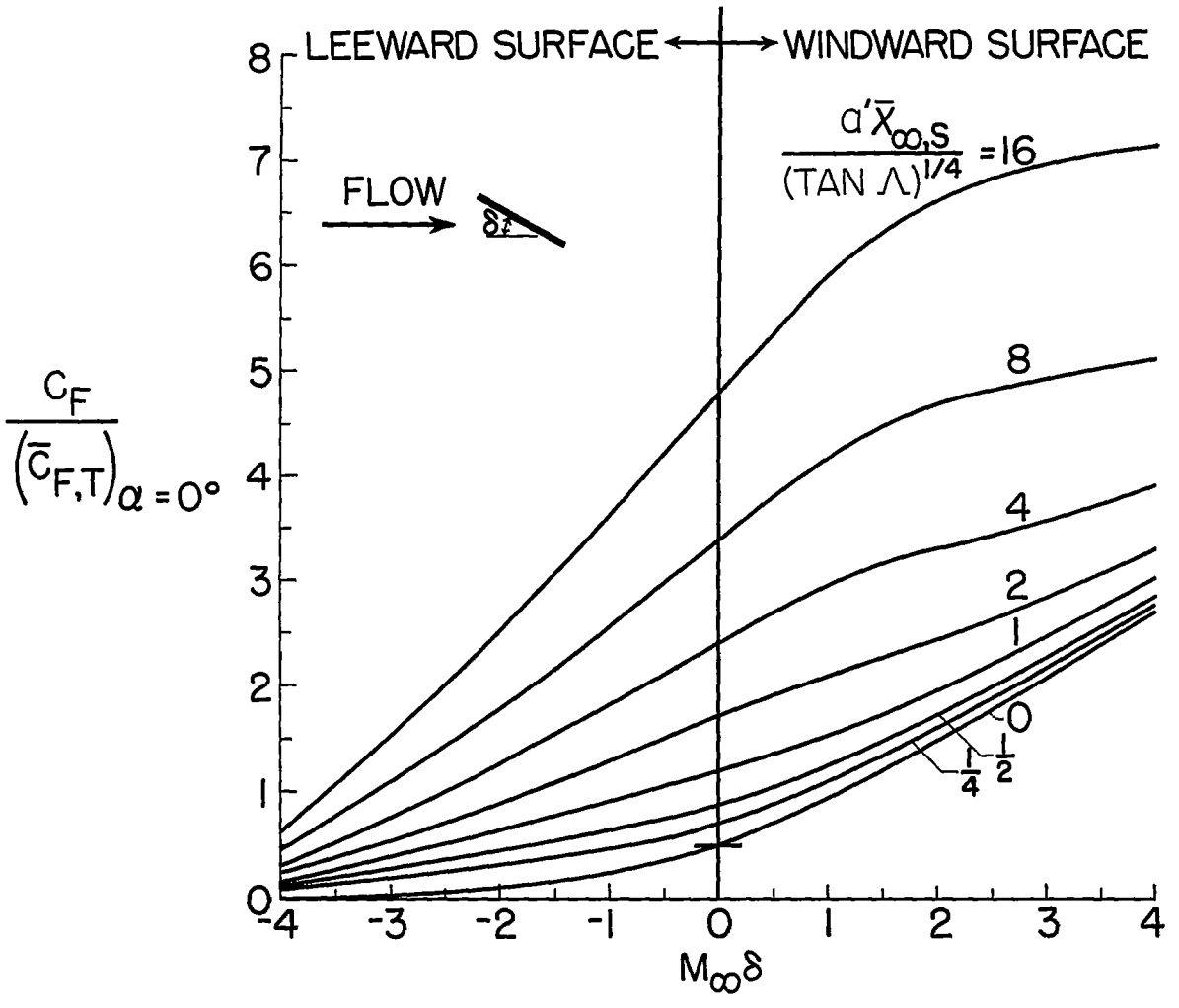

Figure 3.- Boundary-layer-induced and angle-of-attack effects on skin friction of a delta-plan-form flat plate. $\gamma = \frac{7}{5}$.

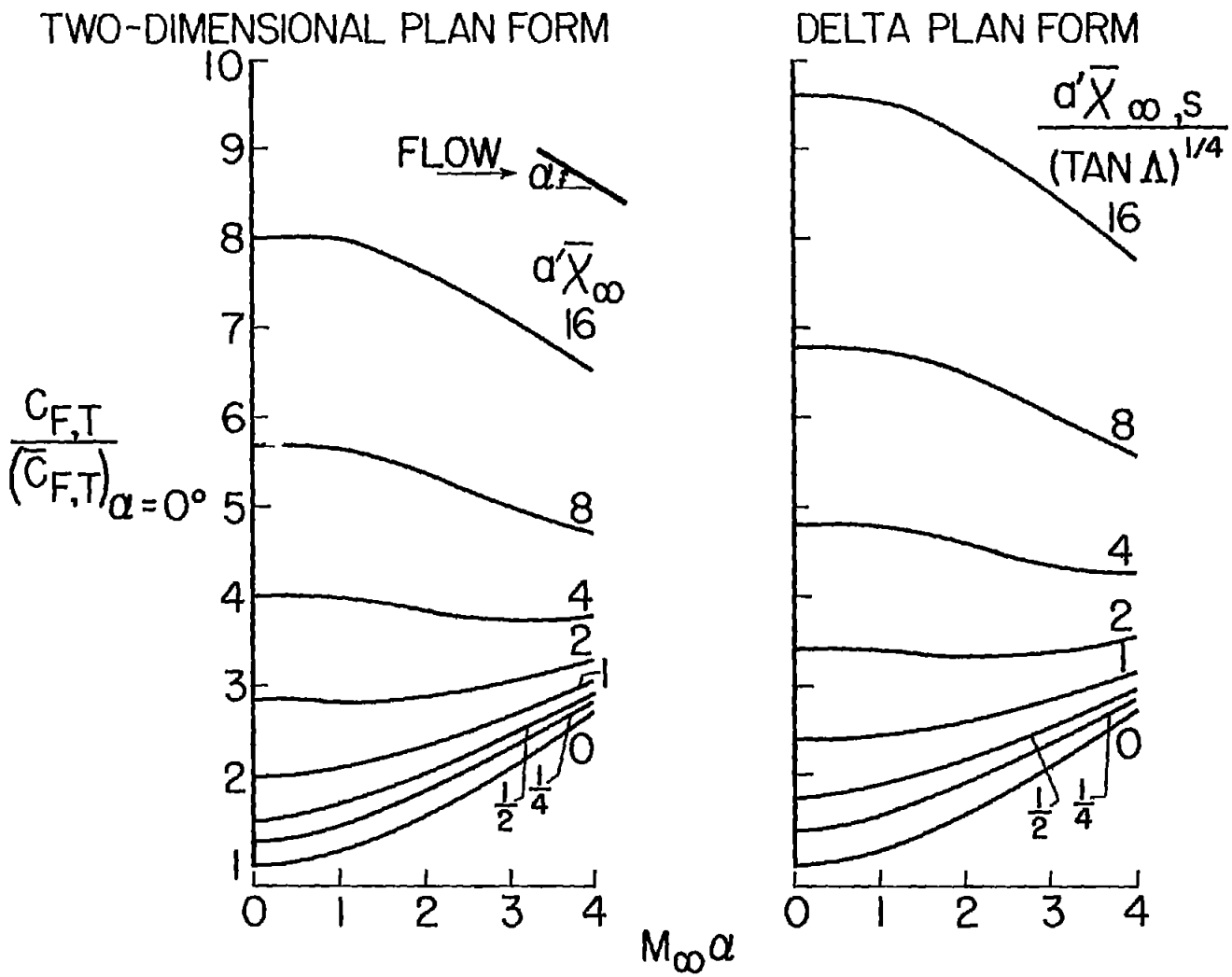

Figure 4.- Hypersonic boundary-layer-induced and angle-of-attack effects on total skin friction of flat plates. $\gamma = \frac{7}{5}$.

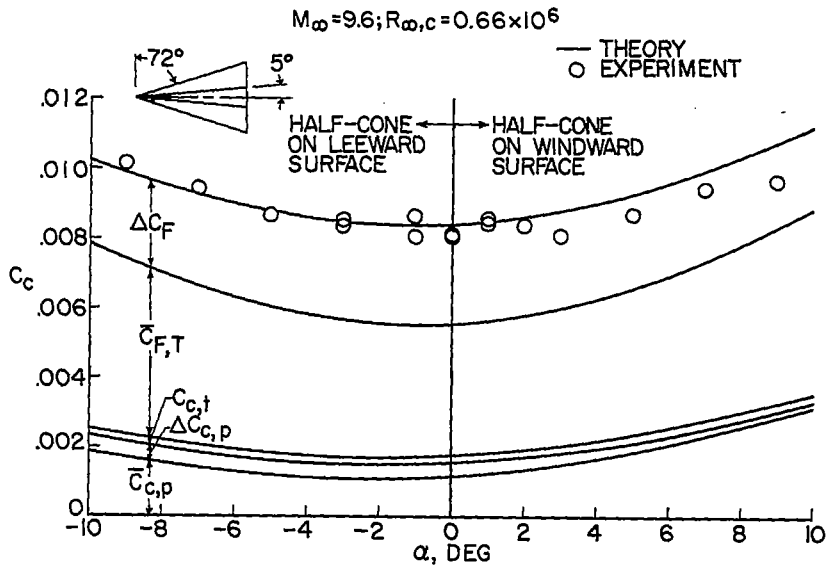

Figure 5.- Chord force for delta-wing—half-cone combination tested in air.

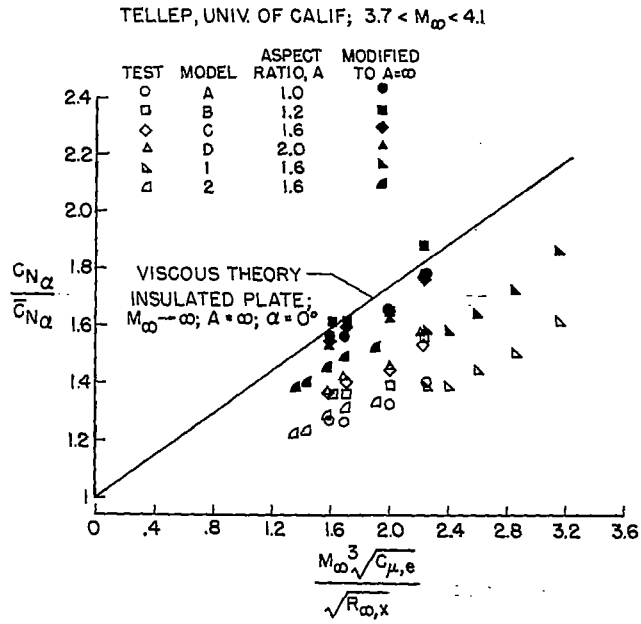

Figure 6.- Effect of viscous interaction and aspect ratio on C_{N_α} of rectangular wings tested in air.

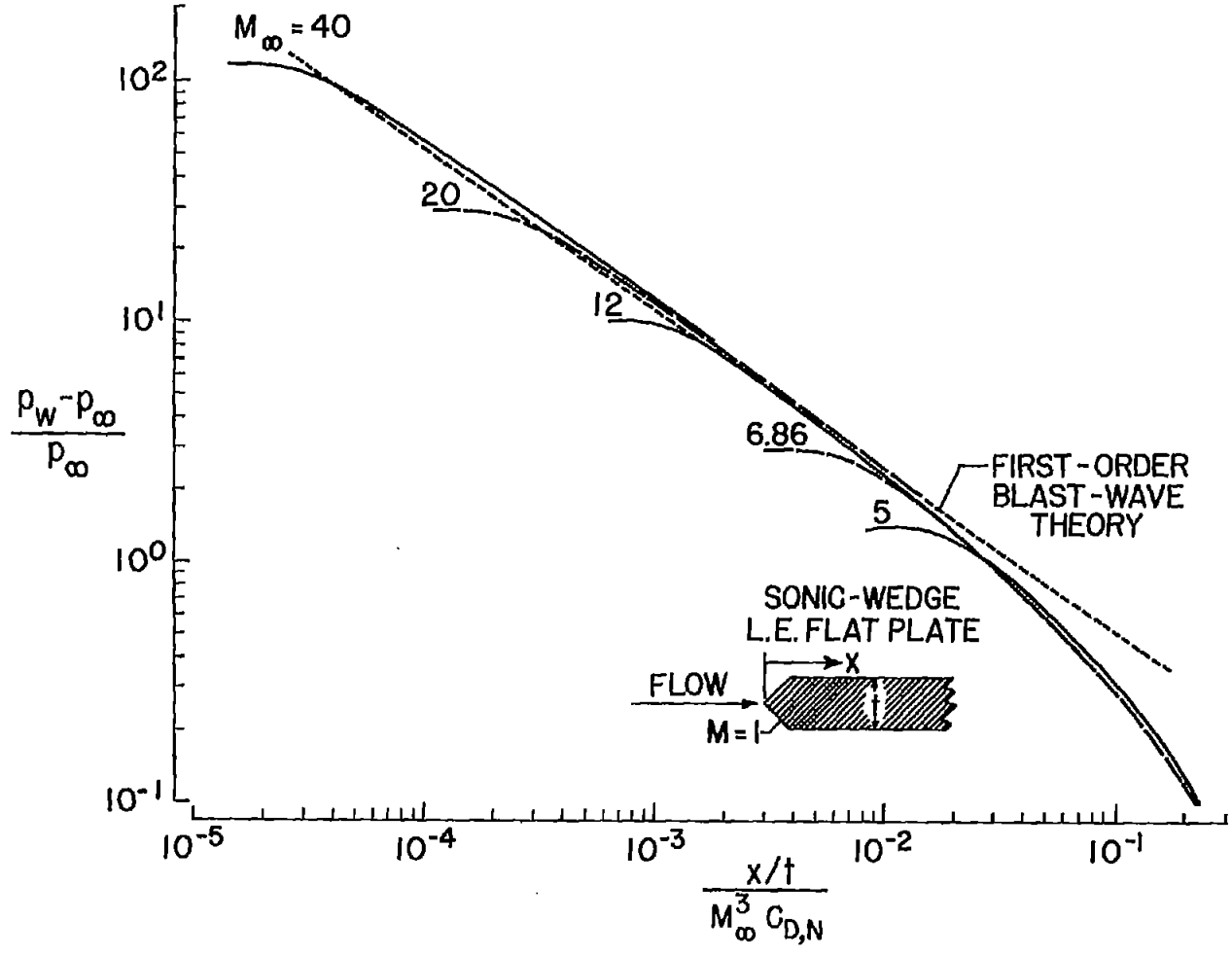

(a) $\gamma = \frac{7}{5}$.

Figure 7.- Correlation of pressures induced by blunt leading edge. $\alpha = 0^\circ$; $\Lambda = 0^\circ$.

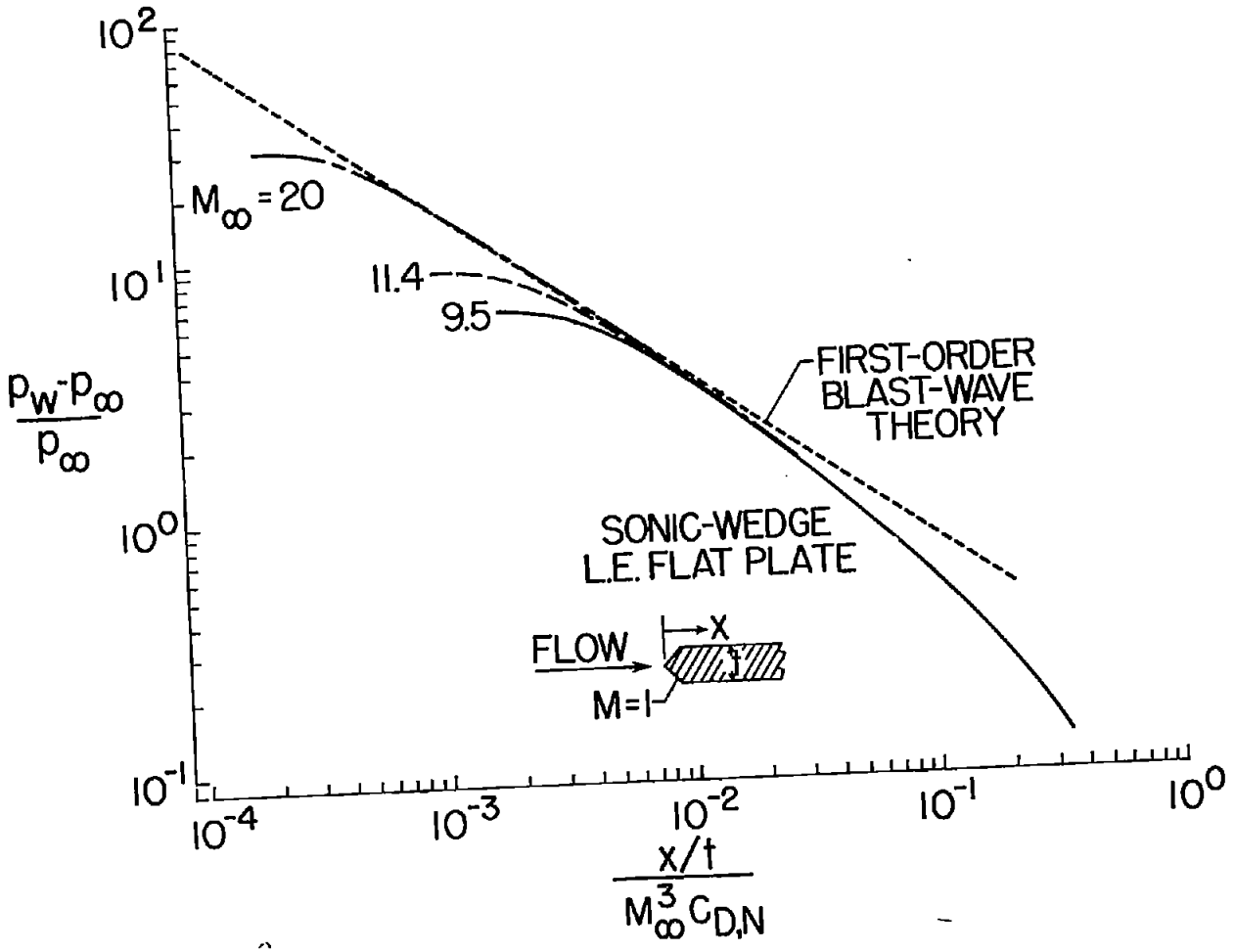

(b) $\gamma = \frac{5}{3}$.

Figure 7.- Concluded.

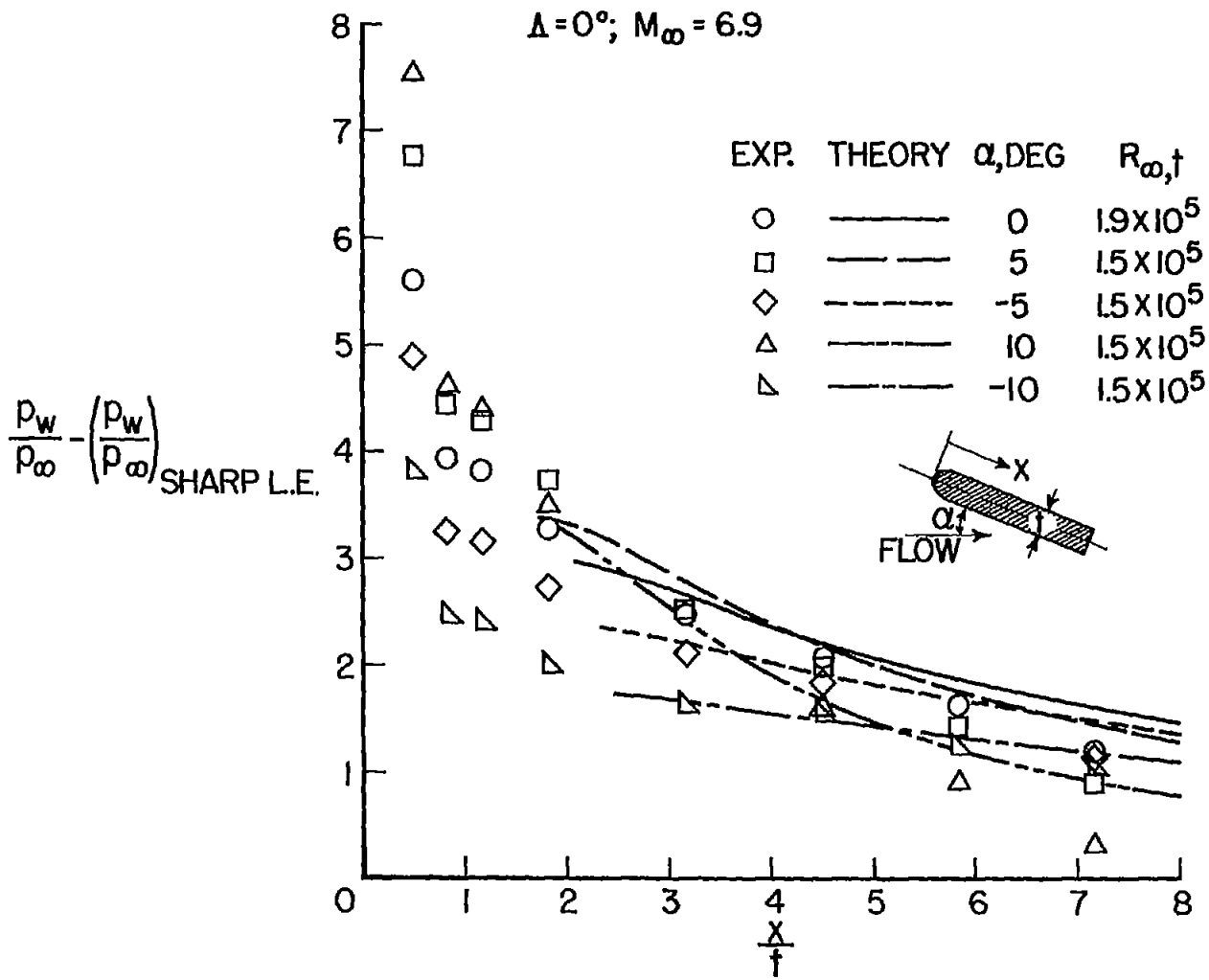

Figure 8.- Effect of α on flat plate with blunt leading edge tested in air.

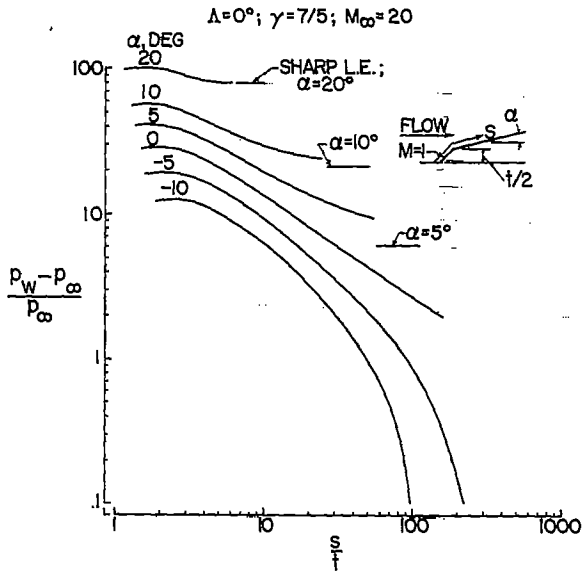

Figure 9.- Effect of α on blunt-leading-edge induced pressures on a flat plate.

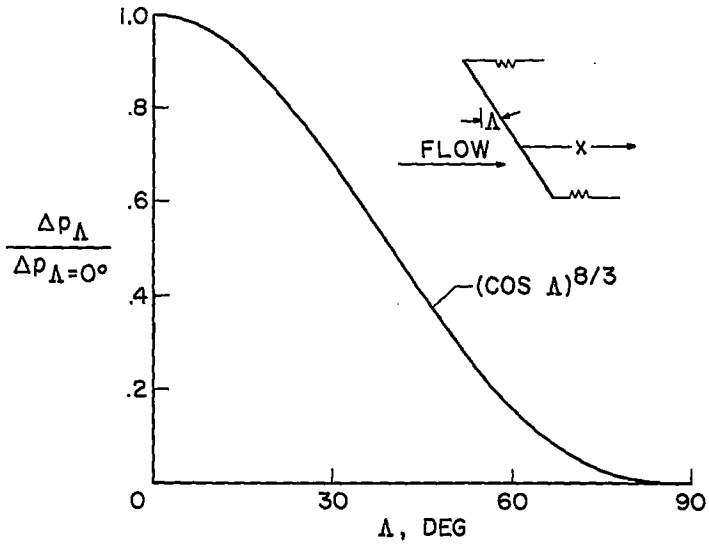

Figure 10.- Effect of leading-edge sweep on blunt-leading-edge induced pressures. $\alpha = 0^\circ$.

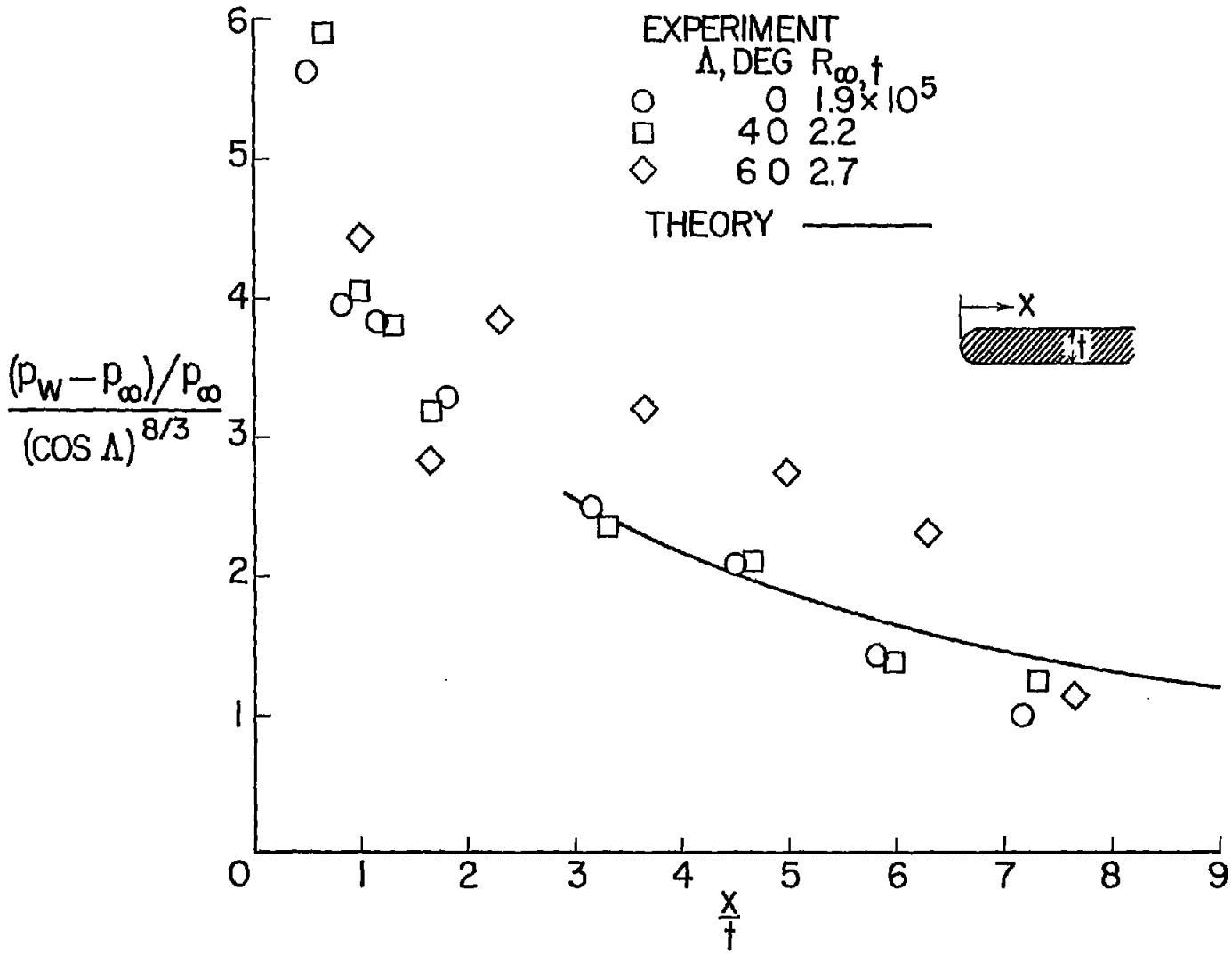

Figure 11.- Correlation of pressures on a flat plate with a hemicylinder leading edge tested in air. $\alpha = 0^{\circ}$; $M_{\infty} = 6.9$.

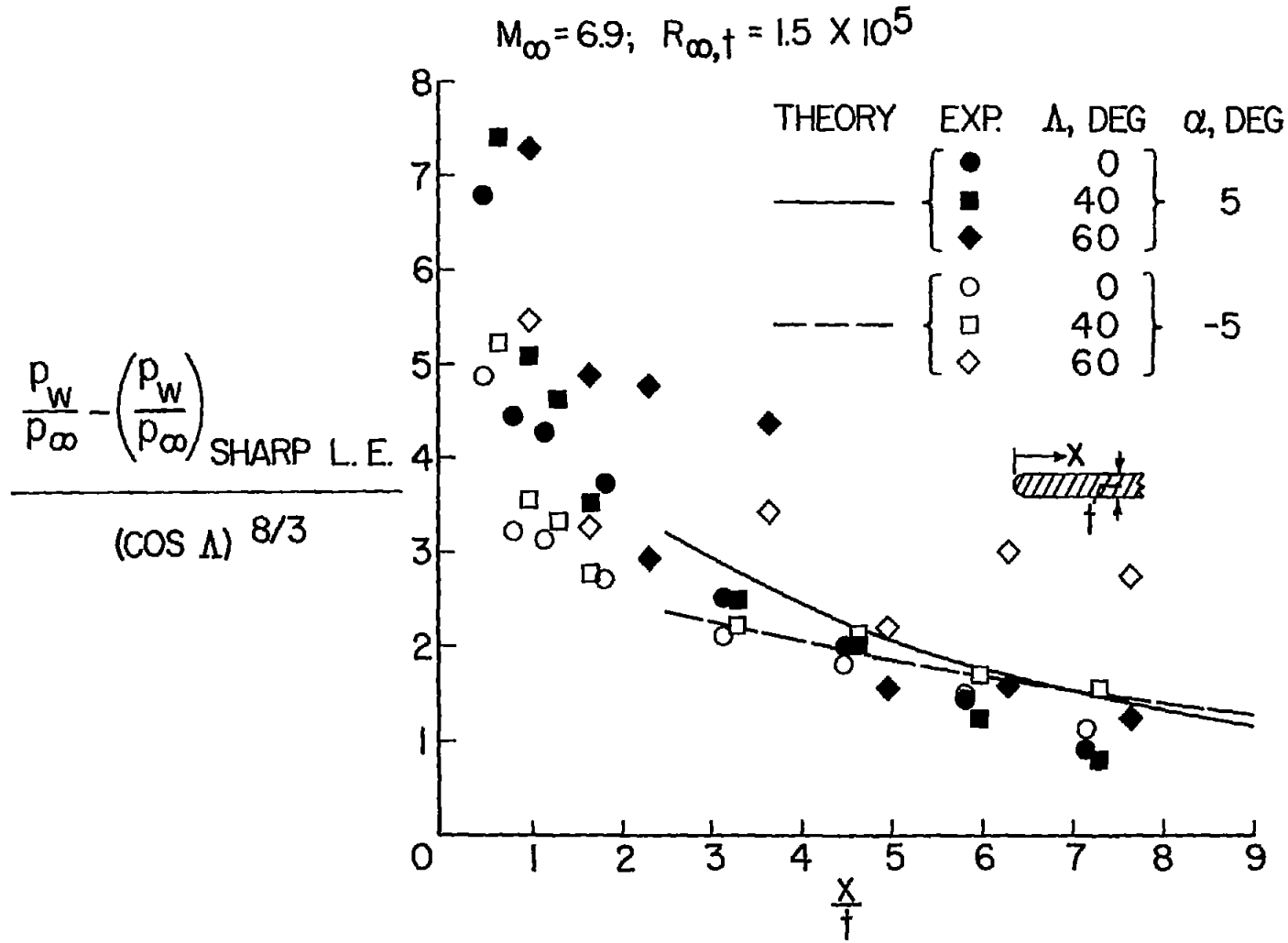

Figure 12.- Effect of sweep on pressures on a flat plate with hemicylinder leading edge tested in air.

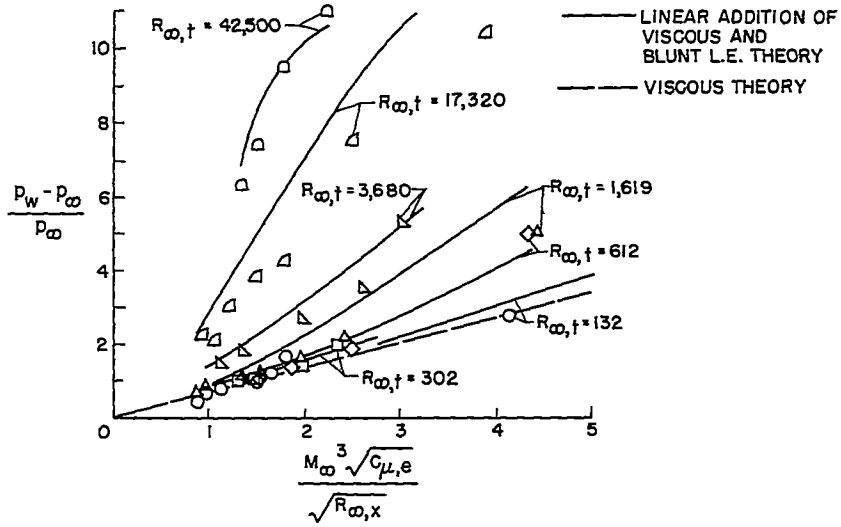

(a) Princeton helium tunnel; M_∞ = 11.4.

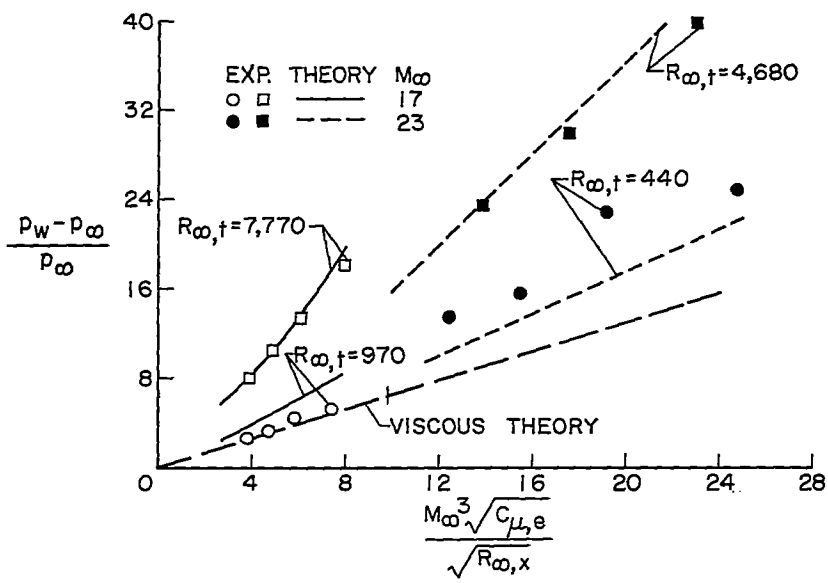

(b) Langley 2-inch helium jet.

Figure 13.- Combined viscous and leading-edge bluntness effects on flat-plate pressures.

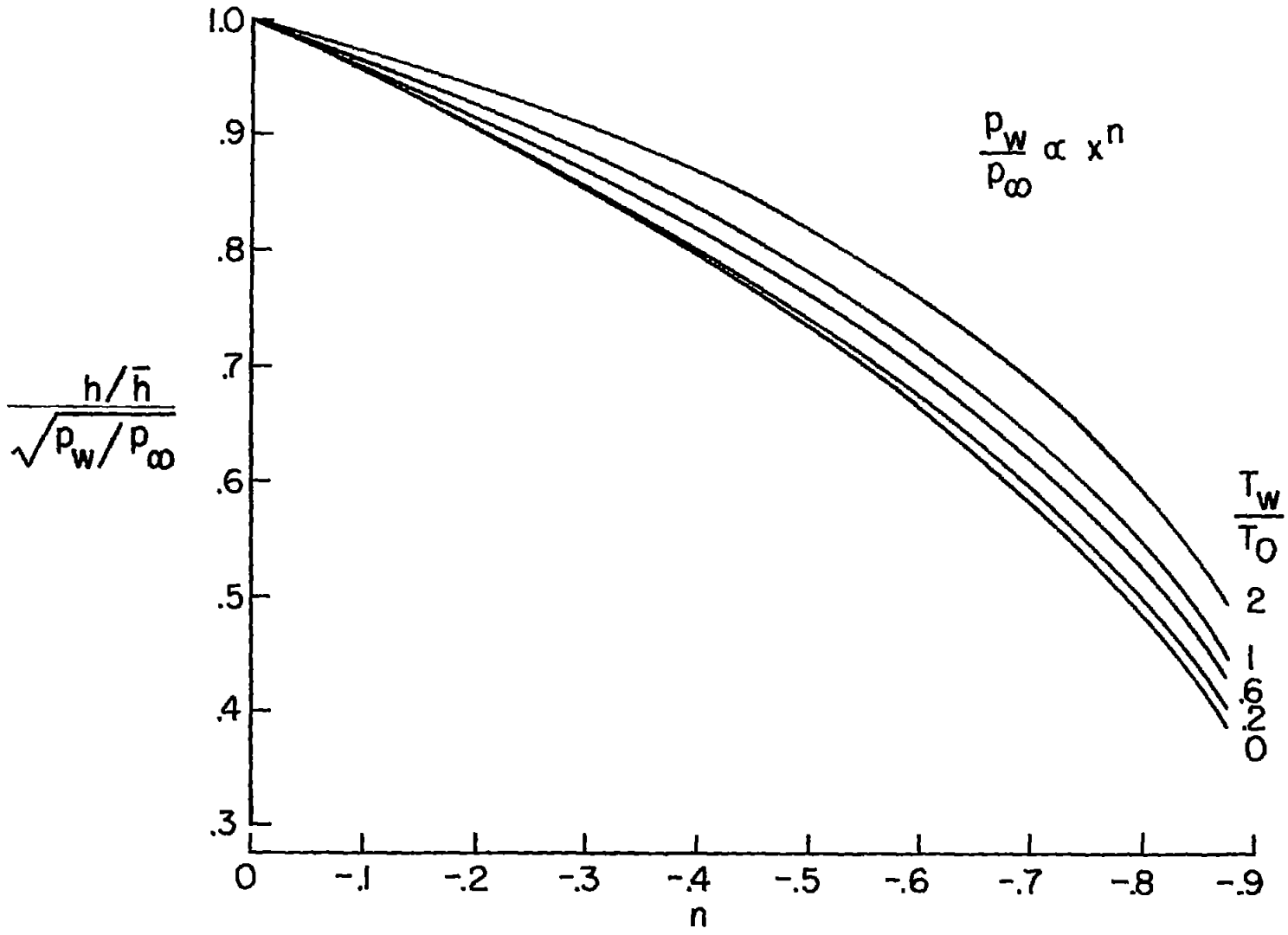

Figure 14.- Effect of favorable pressure gradients on heat transfer by method of similar solutions for hypersonic flow. $\gamma = \frac{7}{5}$.

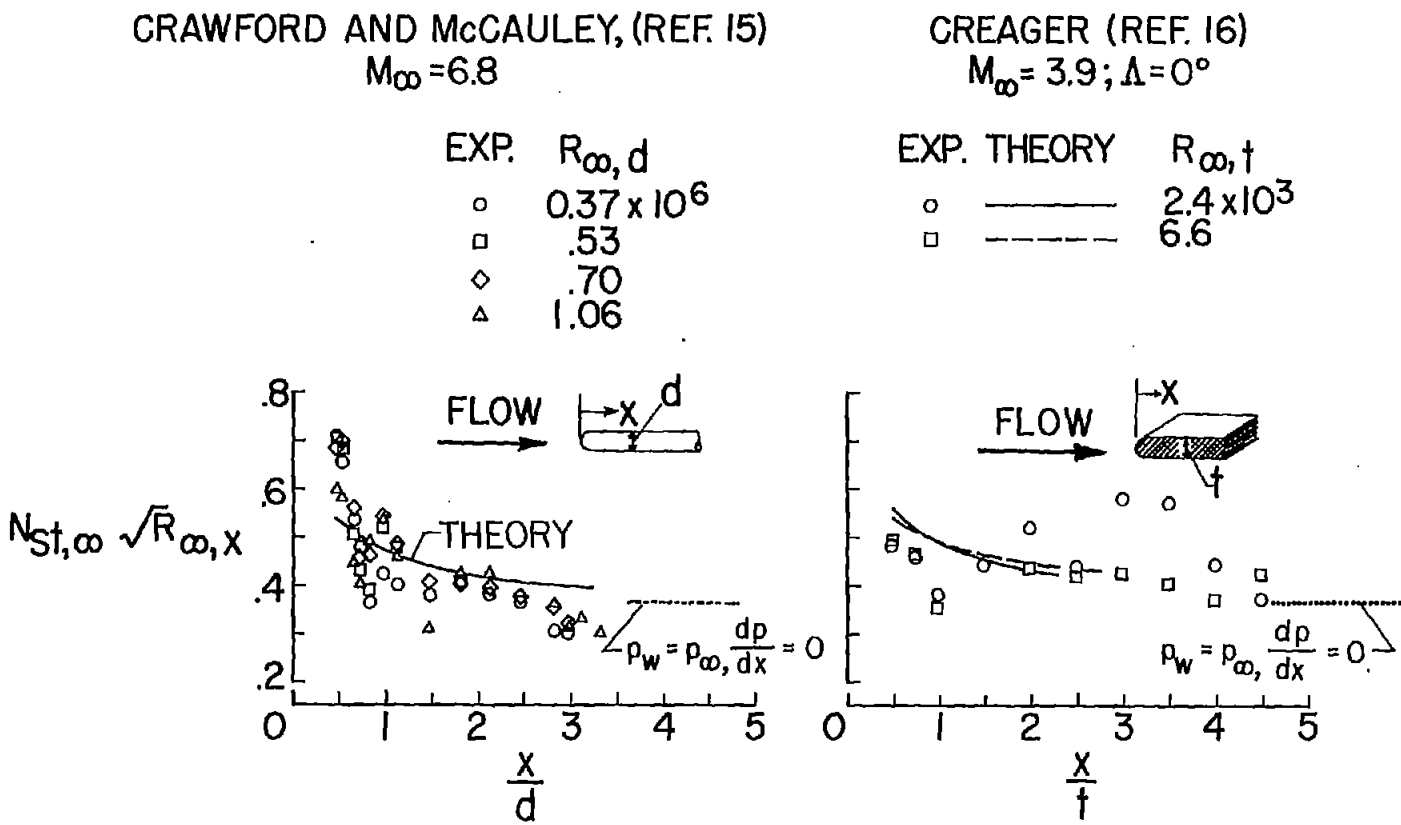

Figure 15.- Heat transfer to a blunted rod and to a blunted flat plate tested in air.

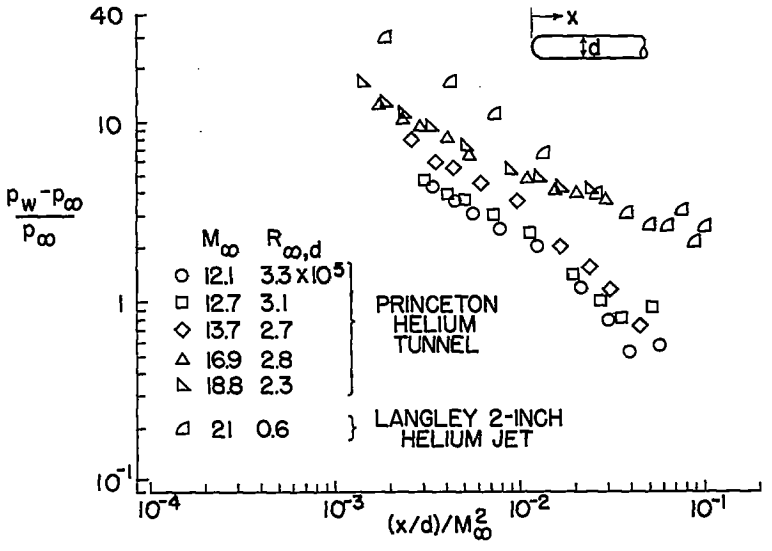

(a) Hemispherical nose.

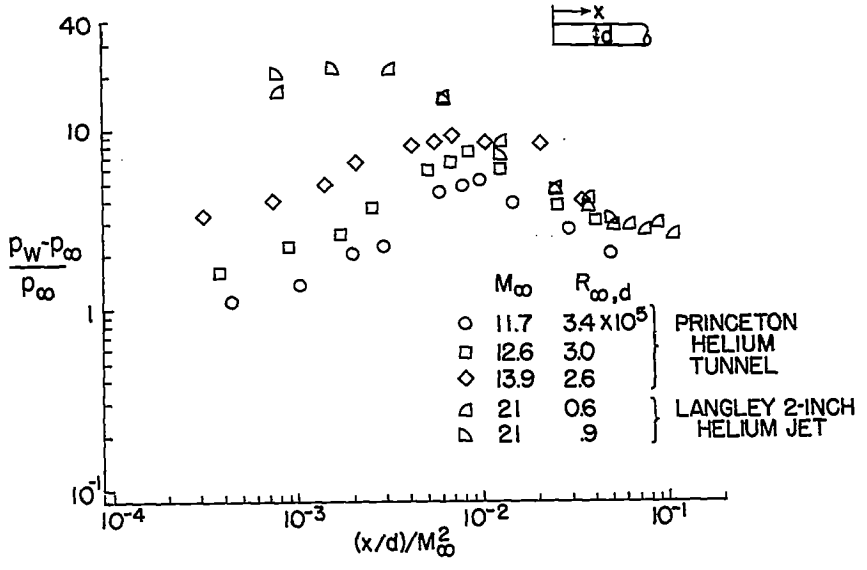

(b) Flat-face nose.

Figure 16.- Pressure distribution on blunted rods tested in helium.

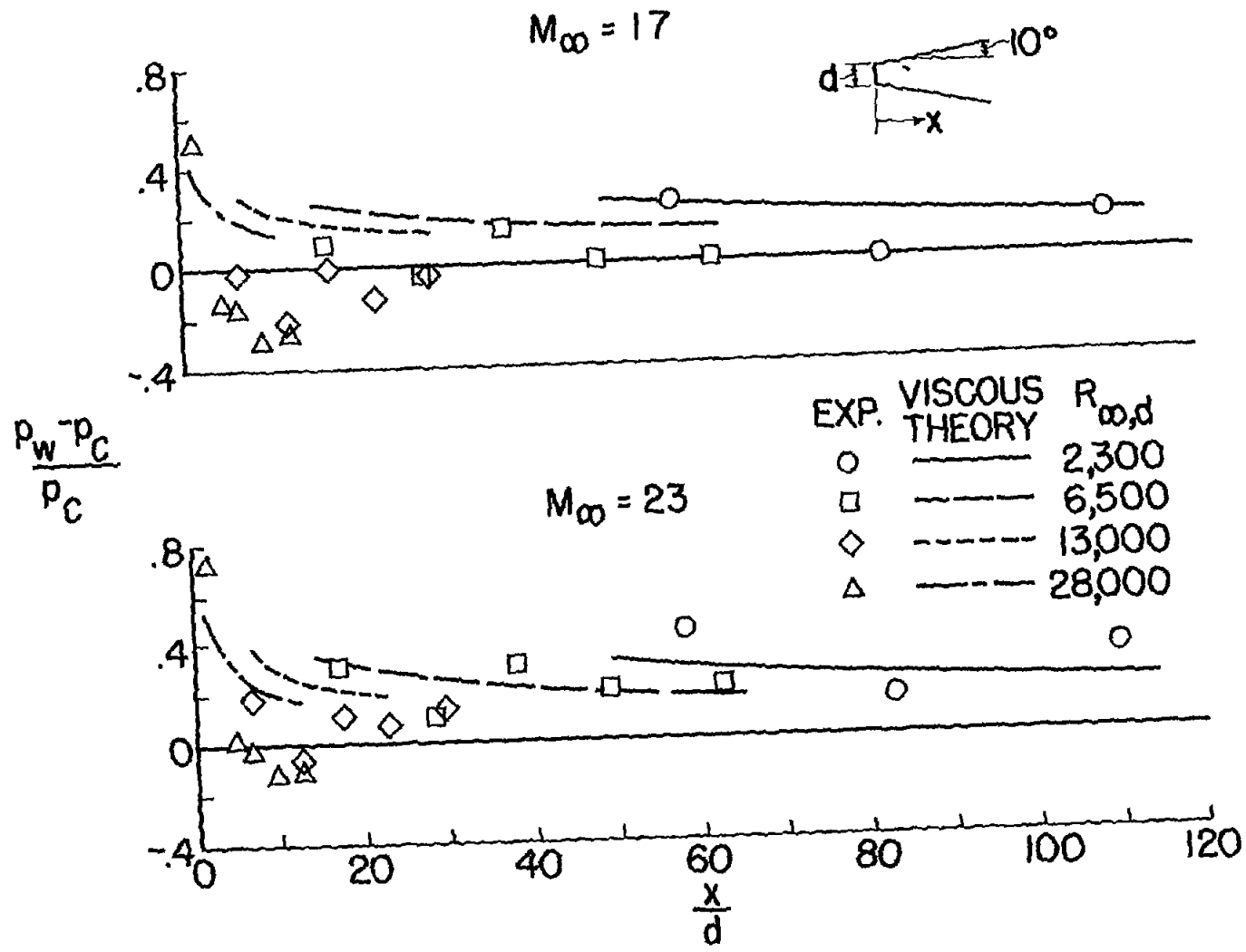

Figure 17.- Pressure distribution on a blunted cone tested in helium.

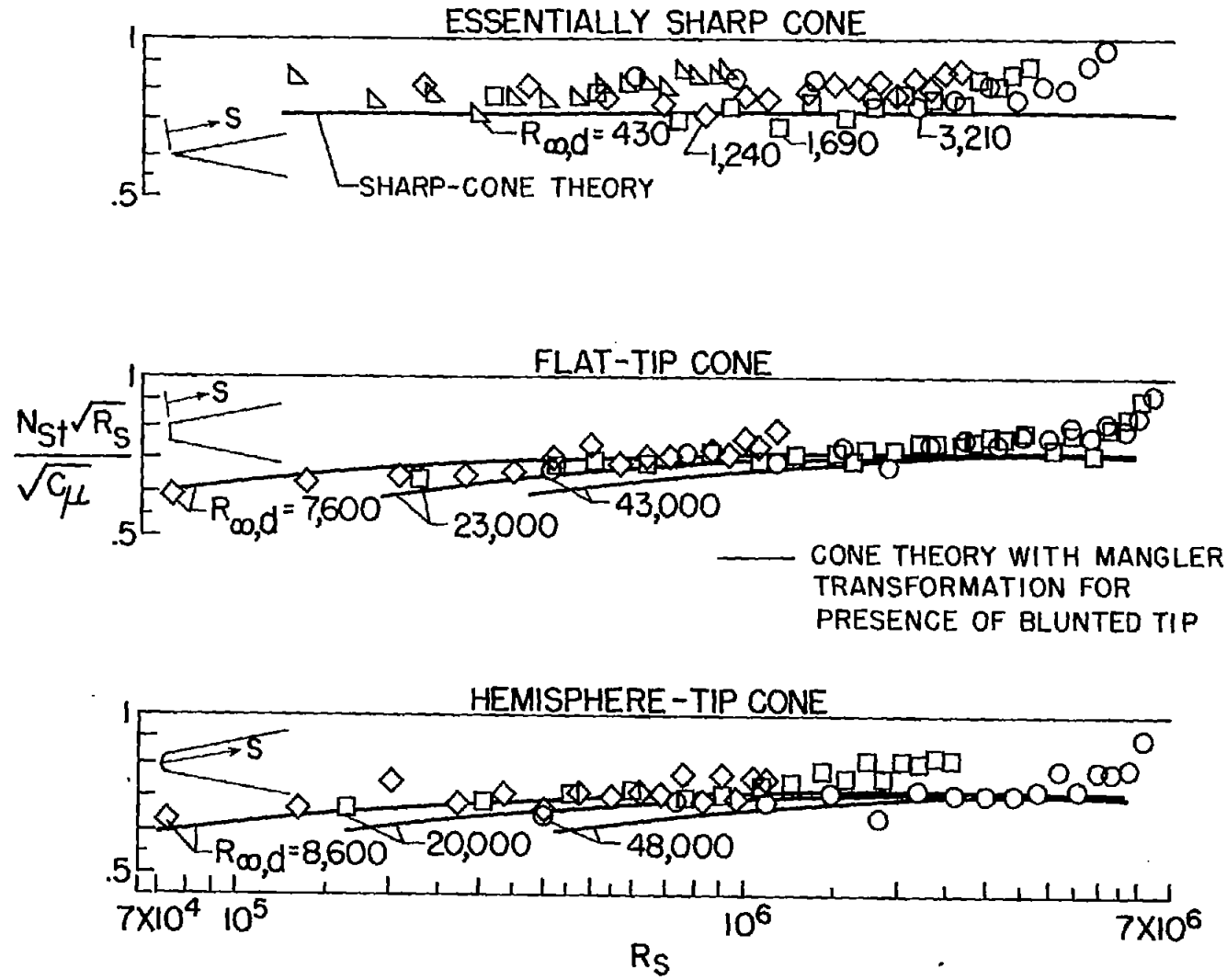

Figure 18.- Heat transfer to sharp and blunted 10° half-angle cones tested in air at $\alpha = 0^\circ$. $M_\infty = 6.7$.

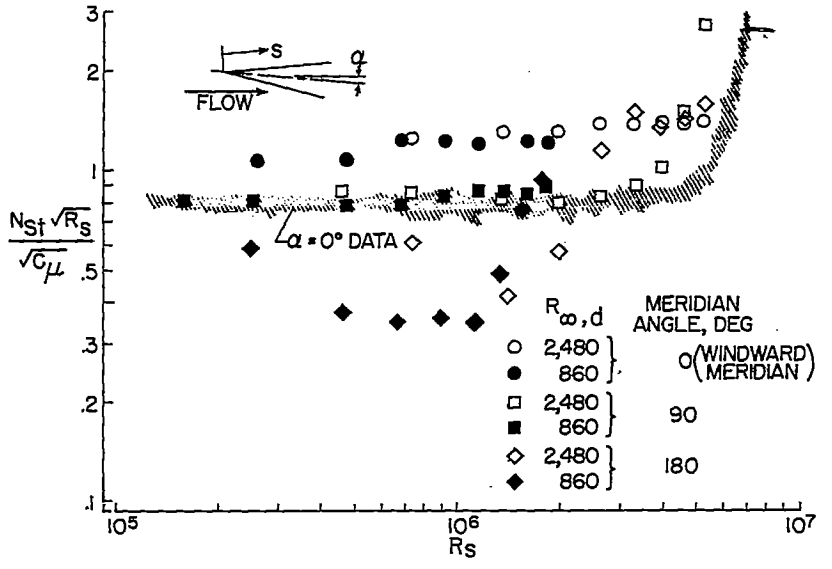

(a) Sharp nose.

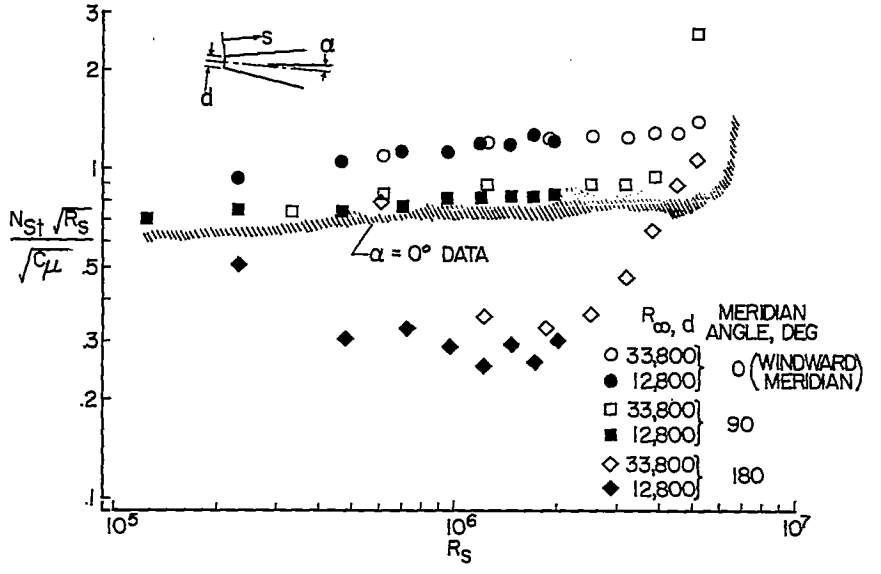

(b) Flat-face nose.

Figure 19.- Heat transfer to sharp and blunted 10° half-angle cones tested in air at $\alpha = 5°$. $M_\infty = 6.7$.